Infrared Characterization of a Micro Turbine Engine Plume

Francisco Sircilli [a], Stephanus Johannes Paulus Retief [b], Luciano Barbosa Magalhães [c], Luty Rodrigues Ribeiro [d], Ademilson Zanandrea [e], Cornelius Brink [b], Maikon Nascimento [e], Maria Magdalena Dreyer [b]

[a] Instituto de Estudos Avançados, Brazil; [b] Denel Dynamics, South Africa; [c] Comando-Geral de Operações Aéreas, Brazil; [d] Instituto de Aeronáutica e Espaço, Brazil; [e] Mectron Eng., Brazil.

***Abstract* — Very important issues concerning numerical simulation of infrared scenarios in military applications are the radiometric emission properties of aircraft plumes as well as the engine tail pipes. In this paper, a detailed description of the experimental set-up and some results of the infrared characterization of a micro turbine engine at ground level (having altitude of ~1500 m AMSL) are presented. The main instruments used were a medium wave infrared camera and a spectroradiometer. The radiometric properties were evaluated in three situations: firstly, by varying the aspect angle between the camera's field of view and the turbine's longitudinal axis, while maintaining a fixed engine velocity of rotation; secondly by varying this velocity for fixed aspect angle and, finally, for a small spectroradiometer field of view when observing three different points along the plume. The engine's infrared numerical model, based on its observed infrared radiometric properties, is intended to be inserted in infrared scenario simulation software.**

***Key words* — infrared scenarios, plume, turbine.**

I. INTRODUCTION

Infrared (IR) scenario modeling and simulation software is a tool that allows experimentation with IR measures, countermeasures, counter-countermeasures etc. in military applications. Such a simulation is significantly cheaper than applying only the method of hardware/software development followed by field testing. Although the final performance of an IR device must be evaluated in a field test, extensive use of hardware and software simulations before the expensive build and break experimentation can reduce risk, lower cost and shorten development time scales [1]. Moreover, a modeling and simulation approach provides a deep understanding of the physics and engineering phenomena involved, which result in a solid opportunity of both refinement and improvement of the IR device.

Input data for this kind of software are geometric and IR radiometric properties of all elements involved, such as shapes, sizes, distances, radiances and intensities, including a sufficiently accurate terrain background. Among this data, very important aspects concerning the numerical simulation of IR scenarios are the plume radiance of the aircrafts as well as the radiometric properties of their engine tail pipes.

This work presents the radiometric IR properties measured at ground level (having altitude of ~1500 m AMSL) of a commercial micro turbine engine's plume. Although this engine is normally intended to thrust airplane models and is not used in real aircraft, the methods of measurement and data reduction are valid so that they can be applied directly in the real world to a real aircraft plume. Although a real aircraft's plume has larger dimensions than the micro turbine's plume, the temperatures involved cover the same range, and the identical fuel (Jet A-1) used by real aircraft is used by this micro turbine. The work presented here was an outcome of a training course given by the South African authors of this paper.

The basic instrumentation available and appropriated for these plume measurements were a Medium Wavelength Infrared (MWIR) camera operating in the 3.6 μm to 5.1 μm spectral range and a FTIR (Fourier Transform Infrared) spectroradiometer (SR) operating in the 0.8 μm to 5.5 μm spectral range. Complementary instrumentation, such as a portable weather station, an extended area blackbody, a time synchronizer and a GPS antenna, were also deployed.

The radiometric properties of the micro turbine plume were evaluated considering three measurement sessions during which a specific parameter of interest were adjusted: varying the turbine velocity of rotation (RPM) for a fixed aspect angle of 90 degrees between the MWIR's field of view (FOV) and the longitudinal axis of the turbine (called RPM scan session in this paper); varying the aspect angle (AA) for a fixed RPM (called AA scan session in this paper); and, finally, for a small SR FOV looking at three positions along the plume for a fixed RPM and aspect angle (called small FOV session in this paper).

The engine was mounted on a bench, which allowed changing of the aspect angle in the AA scan session of measurements as well as allowing secure controlling of the engine velocity during the measurements.

For further continuity of this work, all the radiometric data obtained will be submitted to a data reduction process and it will furthermore be used to create a computerized mathematical model. This model will be implemented in infrared scenario simulation software.

Some theoretical considerations are presented in section II, the experimental set-ups for the three measurement sessions are described in section III, some results obtained are shown in section IV and conclusions are supplied in section V.

II. THEORETICAL CONSIDERATIONS

Contributions to the infrared signal observed by instrumentation when horizontally directed towards a target

situated at a distance *r*, will usually consist of, but are not necessarily limited to, the following spectral sources (wavelength represented by λ) [2]:

- the absolute target radiance, $L_{trg}(\lambda)$, which can be represented by a blackbody (BB) radiator, $L_{BB}(\lambda)$, at a specific temperature, T, and a specific emissivity associated with the target, $\varepsilon_{trg}(\lambda)$, i.e. $L_{trg}(\lambda,T) = L_{BB}(\lambda,T)\cdot\varepsilon_{trg}(\lambda)$, attenuated by the atmosphere;
- the background radiance, $L_{bkg}(r,\lambda)$, whenever the target is semi-transparent, attenuated by the target as well as the atmosphere;
- the environmental foreground radiance, $L_{frg}(r,\lambda)$, as reflected against the target and then attenuated by the atmosphere;
- the atmospheric path radiance, $L_p(r,\lambda)$ for $r\rightarrow 0$, i.e. thermal emission of the air in the direction from the target towards the camera.

From a phenomenological point of view, taking cognizance of the above mentioned contributions for the case of horizontal measurement through the atmosphere, the following measurement equation can be constructed:

$$L^{meas}(r) = \int_{\lambda_1}^{\lambda_2} L_{BB}(\lambda,T)\cdot\varepsilon_{trg}(\lambda)\cdot\tau_{atm}(r,\lambda)\cdot\tau_{instr}(\lambda)d\lambda + \int_{\lambda_1}^{\lambda_2} L_{bkg}(r,\lambda)\cdot\tau_{trg}(\lambda)\cdot\tau_{atm}(r,\lambda)\cdot\tau_{instr}(\lambda)d\lambda + \int_{\lambda_1}^{\lambda_2} L_{frg}(r,\lambda)\cdot\rho_{trg}(\lambda)\cdot\tau_{atm}(r,\lambda)\cdot\tau_{instr}(\lambda)d\lambda + \int_{\lambda_1}^{\lambda_2} Lp_{r\rightarrow 0}(r,\lambda)\cdot\tau_{instr}(\lambda)d\lambda \quad , (1)$$

where $L^{meas}(r)$ is the measured radiance ($W.m^{-2}.sr^{-1}$) of the target at a distance *r* as observed by a single detector element (pixel) within a staring array camera. Although the radiance of a given object at a given temperature is constant, the functional dependence of the measured radiance on *r* arises due to the atmospheric transmission and emission, which change as a function of this parameter.

The terms on the right in (1) refer to the previously mentioned radiance of the target, to background emission through target, to the environmental emission reflected from target and to atmospheric path radiance, respectively. In these terms:

- the spectral transmittance of the atmosphere is represented by $\tau_{atm}(r,\lambda)$;
- the instrument's spectral response, normalized with respect to the maximum response value within the infrared band of concern, is represented by $\tau_{instr}(\lambda)$. In a general form, considering the optical path through the instrument,

$$\tau_{instr}(\lambda) = \tau_{\det}(\lambda).\tau_{ar}(\lambda).\tau_{lens}(\lambda).\tau_{dewar}(\lambda), \quad (2)$$

where $\tau_{\det}(\lambda)$ refers to the detector's spectral response, and the remaining parameters refer to the spectral transmittances through the anti-reflection coating τ_{ar}, through the lens τ_{lens} and through the dewar window of the detector τ_{dewar};

- $\tau_{trg}(\lambda)$ is spectral transmittance through the target;
- $\rho_{trg}(\lambda)$ is the spectral reflectivity of the target.

The evaluation of Equation (1) in this work is facilitated by using a MatLab script [3].

Depending on the target to be measured, some terms of (1) don't need to be considered. In the case of a plume, the third term on the right (environmental reflection) is not applicable if it is assumed there is no reflection from the plume; also, the fourth term (path radiance) is negligible if the plume was measured over a relatively small distance from the camera. In this way, the resultant plume measurement equation applicable to this study contains only the terms related to the target and background.

Equation 1 can now be solved for $L_{trg}(\lambda)$ by means of a numerical technique if the spectral atmospheric transmittance, spectral instrument response, spectral background radiance and plume spectral transmittance is known. A solution of $L_{trg}(\lambda)$ can however be obtained from wideband estimates of these spectral parameters if use is made of 'effective transmittance' and 'effective response' values, defined as the weighted average over a specified spectral band of the spectral parameter.

The effective wideband transmittance of the background radiance through the plume is

$$\tau_{trg.bkg} = \frac{\int_{\lambda_1}^{\lambda_2} L_{bkg}(r,\lambda)\cdot\tau_{trg}(\lambda)\cdot\tau_{instr}(\lambda)\,d\lambda}{\int_{\lambda_1}^{\lambda_2} L_{bkg}(r,\lambda)\cdot\tau_{instr}(\lambda)\,d\lambda},$$

and further transmittance through the atmosphere of this radiance is described by

$$\tau_{atm.trg.bkg} = \frac{\int_{\lambda_1}^{\lambda_2} L_{bkg}(r,\lambda)\cdot\tau_{trg}(\lambda)\cdot\tau_{atm}(\lambda)\cdot\tau_{instr}(\lambda)\,d\lambda}{\int_{\lambda_1}^{\lambda_2} L_{bkg}(r,\lambda)\cdot\tau_{trg}(\lambda)\cdot\tau_{instr}(\lambda)\,d\lambda}.$$

The effective transmittance of the target radiance itself through the atmosphere is

$$\tau_{atm.trg}(r,T) = \frac{\int_{\lambda_1}^{\lambda_2} L_{BB}(\lambda,T)\cdot\varepsilon_{trg}(\lambda)\cdot\tau_{atm}(r,\lambda)\cdot\tau_{instr}(\lambda)\,d\lambda}{\int_{\lambda_1}^{\lambda_2} L_{BB}(\lambda,T)\cdot\varepsilon_{trg}(\lambda)\cdot\tau_{instr}(\lambda)\,d\lambda},$$

while the effective response of the instrument to the plume spectrum is given by

$$\tau_{instr.trg} = \frac{\int_{\lambda_1}^{\lambda_2} L_{BB}(\lambda,T)\cdot\varepsilon_{trg}(\lambda)\cdot\tau_{instr}(\lambda)\,d\lambda}{\int_{\lambda_1}^{\lambda_2} L_{BB}(\lambda,T)\cdot\varepsilon_{trg}(\lambda)\,d\lambda}.$$

The MWIR data reduction equation (1) for plume wideband radiance, L_{trg}, can now be written as:

$$L_{trg} = \frac{L^{meas} - L_{bkg}(r).\tau_{trg.bkg}(r).\tau_{atm.trg.bkg}(r)}{\tau_{atm.trg}(r,T).\tau_{instr.trg}(T)}, \qquad (2)$$

where $L_{bkg}(r) = \int_{\lambda_1}^{\lambda_2} L_{bkg}(r,\lambda)\cdot\tau_{instr}(\lambda)\,d\lambda$ and $L_{trg}(r) = \int_{\lambda_1}^{\lambda_2} L_{BB}(\lambda,T)\cdot\varepsilon_{trg}(\lambda)\,d\lambda$. Other definitions for the effective wideband parameters can also be used, as long as the data reduction Equation (2) remains mathematically identical to Equation 1, albeit in a rearranged form. Using the above definitions, however, result in Equation (2) being easy to interpret in terms of the relative contributions and influences of the different mechanisms determining the target radiance.

III. Experimental Set-up

Fig. 1 is a photo of the whole set-up used to measure the engine plume for the specific case of the small FOV session. Indicated from the left to right are the blackbody and table with the turbine engine, the positions of MWIR camera and SR, the portable weather station, the GPS antenna used to synchronize the instrument control computers' time and the mobile lab, which accommodates the computers and other accessories.

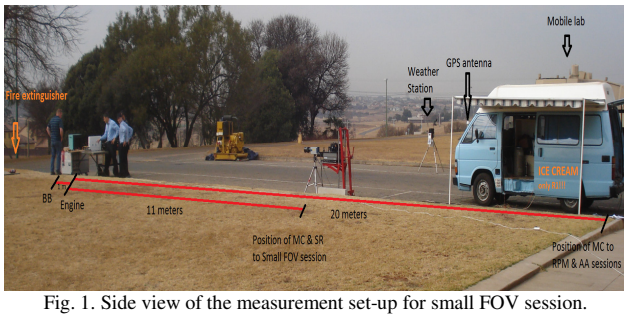

Fig. 1. Side view of the measurement set-up for small FOV session.

The engine used in all three measurement sessions was a commercial Kingtech K80 micro turbine engine mounted on a wooden board, with all components needed to start and control the performance of the turbine, as shown in Fig. 2.

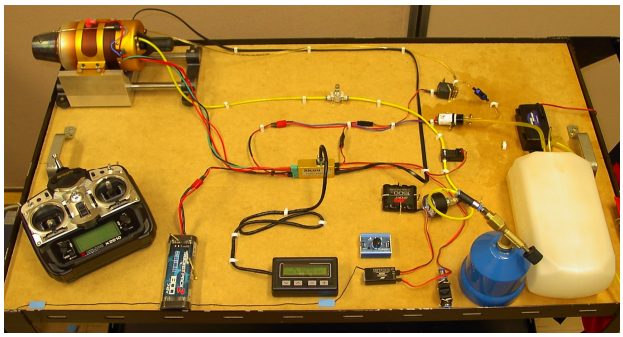

Fig. 2. Engine set-up: fuel tank (white), gas cylinder (blue), turbine itself (at left upper side), data controller (black box with green display), FADEC auto starter (yellow, in the middle), solenoid valves, batteries, actuators and so on.

The engine was started by an injection of a butane/propane gas mixture (typically 40/60) in the turbine, until a stable flame was obtained, followed by the injection of liquid fuel (Jet A-1 with 5% of lubricant additive). When the rotation speed reached about 25000 RPM, the injection of gas was interchanged with that of the Jet A-1 fuel; The rotation speed was then further increased until the desired rotation speed was obtained. The control of rotation could be by two means – a radio remote control, the option used in all measurements, or manually by varying the electrical signal to be sent to the FADEC auto starter.

As the plume signal is weak in the 1 µm to 2 µm spectral range, a camera sensitive in the Short Wavelength Infrared (SWIR) range was not deployed. The SWIR signal is detectable only when the plume gas density is so high that the transmittance goes to zero and the emissivity ($\varepsilon = 1-\tau$) tends to one – then the plume acts like a blackbody. This occurs in the thrust afterburner stage of an aircraft engine [4].

The spectroradiometer has two channels – channel A (Ge detector) operating in the 0.91 µm to 1.72 µm spectral range, and channel B (InSb detector) operating in the 0.83 µm to 5.5 µm range. For the same reason that the SWIR camera was not used, only the InSb detector was used in SR measurements.

In order to synchronize all the instrument recordings, a Masterclock TCR1000 connected to the GPS external antenna was connected to all the instrument control PCs.

For the RPM scan session, only the MWIR camera was used to determine the IR emission of the micro turbine plume at different engine settings. Fig. 3 represents the set-up for this session in which the turbine was maintained at $\theta = 90°$ aspect angle (the angle between the MWIR camera line of sight and the engine longitudinal axis). The distance between the MWIR camera and the engine was 20 meters and it was used without any filter and with a 200 mm lens in order for the plume to fill the MWIR FOV. The measurements were done for 30 µs, 240 µs and 2800 µs integration times. Besides the MWIR images, notes of the actual RPM and temperature values of the engine during the recordings were also taken. The nominal engine rotation values in rotations per minute units were 45k, 60k, 80k, 100k, 110k, 120k, 125k, 130k, 140k and 145k.

In the AA scan session, only the MWIR camera was used to determine the IR emission of the micro turbine plume at different aspects angles, as showed in Fig. 3. The aspect angle θ was varied for angles of 0º, 30º, 45º, 60º, 70º, 90º, 110º, 120º, 135º, 150º and 180º. In Fig. 4 it is possible to see close-up photos of the MWIR camera view for two different aspect angles. For this case, we performed the measurements without filter, which was intended to obtain the plume radiation.

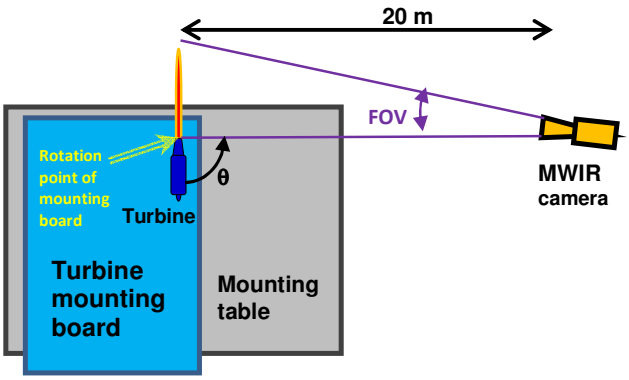

Fig. 3. Plan view diagram of the RPM scan and AA scan measurement sessions.

Fig. 4. View from the MWIR camera line of sight for aspect angles of 135º (left side) and 180º as used in AA scan session.

For the small FOV session, the MWIR camera and the SR were positioned as close as possible to each other, as showed in Fig. 5. The goal of this session was to measure the radiance of the plume and therefore determine the emissivity at three different positions of the plume. In order to have a reference, it was used together with an extended BB at 300°C and a polystyrene board as background, always alternating one of these as the background of the plume. We measured each kind of background for a duration of 5 s. The BB was positioned at 12 m from the MWIR camera and SR, while the polystyrene was temporarily inserted at more or less 11.5 m (a safe distance to avoid melting of the polystyrene). In this session the MWIR camera was configured without filter and a 200 mm lens, while the SR was configured with a 3.5 mrad FOV lens having a 0.8 mm aperture.

Fig. 6 and Fig. 7 show a diagram and a close-up picture of the mounted table, indicating the 3 positions where radiometric parameters were measured: the central points are 30 mm, 185 mm and 340 mm from the border of the tailpipe for the named points A, B and C, respectively. The SR's FOV diameter was 35 mm for the three cases.

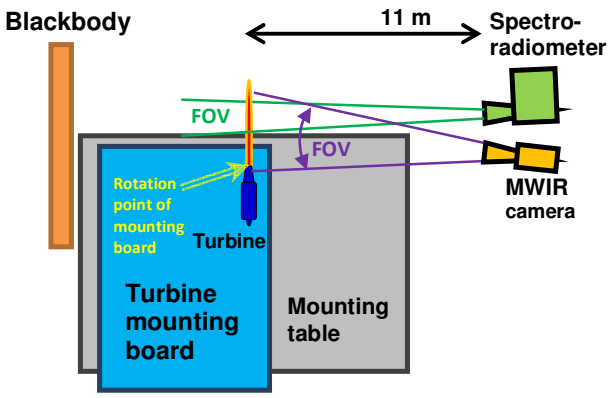

Fig. 5. Plan view diagram of small FOV set-up.

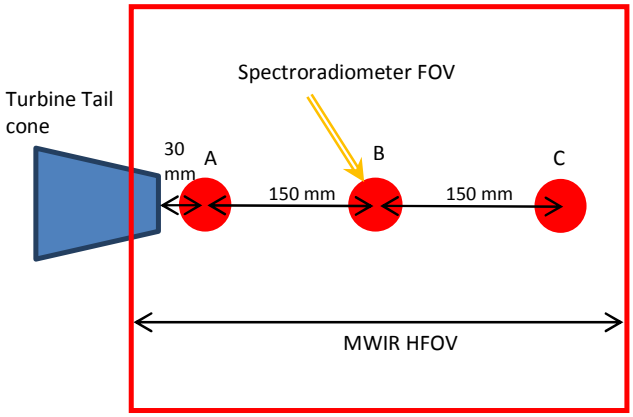

Fig. 6. Diagram used to adjust FOV position of the SR.

Fig. 7. Close-up of the mask used as reference to adjust the three FOV positions of the SR in the small FOV session.

IV. RESULTS

A direct thermocouple measurement in the RPM scan session was taken of the exhaust gas temperature, normally known as EGT, and the engine pump power as shown in Fig. 8. In this figure it can be noted that the EGT is around 450 ºC to 650 ºC for the evaluated range of engine velocity of rotation.

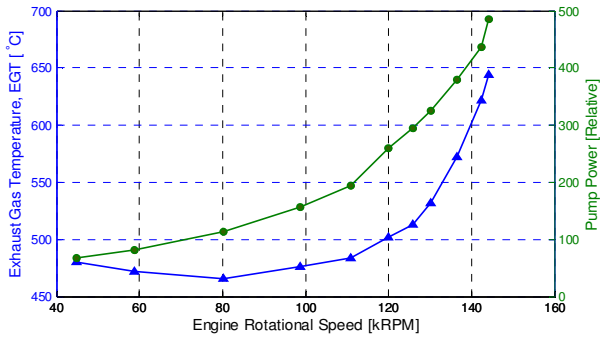

Fig. 8. EGT and pump power as function of engine velocity of rotation.

Figure 9 shows MWIR camera images taken during the RPM scan session, for two engine velocities of rotation: 45 and 145 kRPM. A direct comparison of the two images on face value is not possible because of different display settings (auto-gain, image scaling, etc.) used in order to optimize the image display.

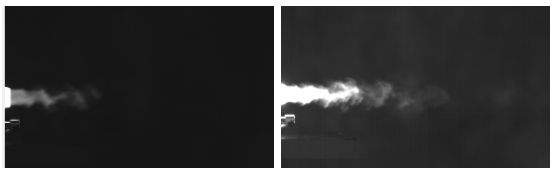

Fig. 9. Plume recordings in the MWIR band at two different RPM engine measurements: 45k RPM (left) and 145k RPM, both for 90° aspect angle.

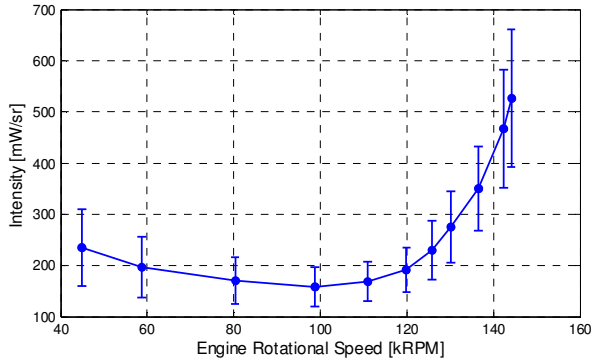

Fig. 10. Plume intensity [W/sr] in MWIR band as function of the Engine Rotational Speed [RPM].

In order to obtain the intensity (W/sr) of the plume for the various cases of the RPM scan session, shown in Fig. 8, the first step was to create an average radiance image using some sequential MWIR images taken during a specific RPM setting. Two others images with average plus and minus standard deviation were created. From the plume radiance and the area filled in an image by the plume, an intensity (product of mean radiance and area) can be calculated. The intensities of the mean and mean ± standard deviation images were calculated, which resulted in the average intensity (blue curve) and its variation (error bars) as shown in Figure 10. The intensity decreases slowly from 45 kRPM until about 100 kRPM, which is a minimum value of the graph, and grows hugely after that as the design speed of the turbine is reached.

Fig. 11 and Fig. 12 show MWIR camera images for two different aspect angles taken to evaluate the plume and tailpipe. The difference between these figures is the filter choice in each situation; in the first set-up no filter was used, while in the second set-up a 4% Neutral Density Filter (NDF) filter was used in order to avoid saturation of the MWIR camera in the geometrical 'hotter' region of the engine tail pipe. This two-fold procedure allows operating in the desired linear region of the MWIR camera detector, without detector saturation in the tail pipe recording or a low signal to noise ratio for the plume recording.

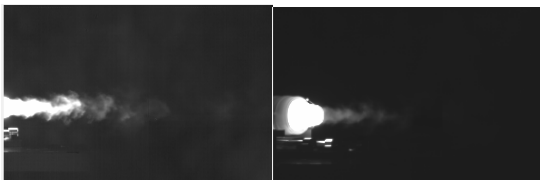

Fig. 11. Plume recording in the MWIR band for 90º (left) and for 135º aspect angles, both for 145 kRPM. No filter was used in order to have the plume radiance well above the detector noise level.

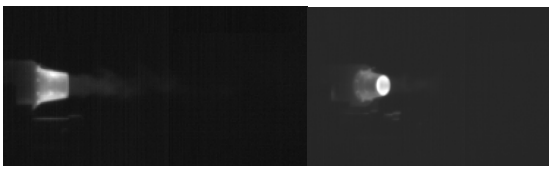

Fig. 12. Tail pipe recordings in the MWIR band for 90º (left) and at 135º aspect angles, both for 145k RPM. A 4% NDF filter was used in order to have no saturation in the tail pipe pixels.

Fig. 13 shows a SR curve obtained for a given measurement in the small FOV session. This curve was derived from an interferogram measured by the FTIR SR, obtained by converting it to a raw spectra followed by calibration in order to obtain radiance values. In this figure it can be noted that there is mostly instrumentation noise in the region of about 1µm to 3 µm (SWIR region), because of limited sensitivity of the InSb detector of the SR in this wavelength region, as well as a weak source signal from the plume in this region (Kintech emission similar to 100% dry setting of aircraft engine as oppose to an afterburner setting); the significant portion of measured spectra is in the MWIR region, as mentioned earlier in this paper. The spectrally selective emission (in the region of 4.2 µm) exhibited in Fig. 13 is to be found in the plume of a full scale aircraft, in which identical combustion processes take place. This emission is the result of a transition between two energy levels of the CO_2 (Carbon dioxide) molecule.

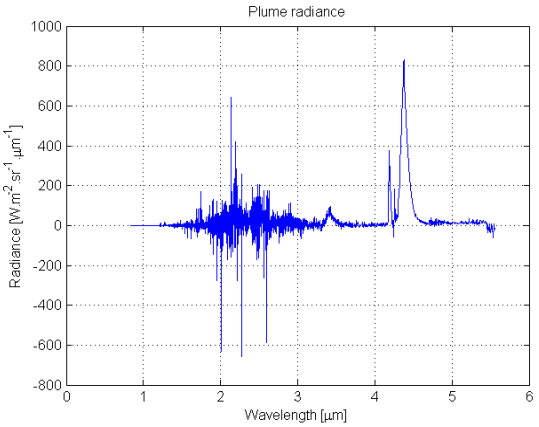

Fig. 13. Measured spectral radiance by SR for 145 kRPM and 90º aspect angle in the small FOV session.

V. CONCLUSIONS

This paper presents a detailed description of the set-up and instrumentation parameters used to measure radiometric properties of a micro turbine engine plume. Although this kind of engine is not used in real aircraft, the methods of measurement and data reduction can be applied similarly in the actual world.

Partial results show that engine EGT is around 450 ºC to 650 ºC in the RPM range evaluated (agreeing with actual full scale aircraft engines) and that a significant portion of SR measured spectra is in the MWIR region. Also shown is the care that was taken in choosing the set-up parameters of the MWIR camera in order to obtain appropriate images.

More results regarding each engine measurement, i.e. radiance, emissivity, transmittance and plume area will be available in a future paper, including data of the tail pipe.

REFERENCES

[1] WILLERS, C. J., "Electro-Optical System Analysis and Design: A Radiometry Perspective", SPIE Press, p. 385, 2013.

[2] RETIEF, S. J. P., SMIT, P. and DREYER, M. M. "Mid-wave infrared characterization of an aircraft plume", Proc IEEE Saudi International Electronics, Commun. and Photonics Conference (SIECPC), 2011.

[3] RETIEF, S. J. P. Cedip_dr.m version 2012-09-11, 2012 (unpublished).

[4] HUDSON, R. D., [Infrared system engineering], John Wiley & sons, New York, (1969).